EUROPEAN ORGANIZATION FOR NUCLEAR RESEARCH

CERN-PPE/92-135
05.08.1992

Production of $f_2(1270)$ and $f_0(975)$ mesons by photons and hadrons of energy 65-175 GeV

The OMEGA Photon Collaboration

R. J. Apsimon[5], M. Atkinson[3], M. Baake[1], L. S. Bagdasarian[7], D. Barberis[2], T. J. Brodbeck[4], N. Brook[3], T. Charity[4], A. B. Clegg[4], P. Coyle[3], S. Danaher[6], S. Danagulian[7], M. Davenport[2], B. Dickinson[3], B. Diekmann[1], A. Donnachie[3], A. T. Doyle[3], J. Eades[2], R. J. Ellison[3], F. Fiedler[1], P. S. Flower[5], J. M. Foster[3], W. Galbraith[6], P. I. Galumian[7], C. Gapp[1], F. Gebert[1], G. Hallewell[5], K. Heinloth[1], R. C. W. Henderson[4], M. T. Hickman[4], K. C. Hoeger[1], R. P. Hofmann[1], A. Holzkamp[1], S. Holzkamp[1], R. E. Hughes-Jones[3], M. Ibbotson[3], H. P. Jakob[1], D. Joseph[1], N. R. Keemer[4], J. Kingler[1], G. Körsgen[1], S. D. Kolya[3], G. D. Lafferty[3], H. M^{C}Cann[3], R. M^{C}Clatchey[2], C. M^{C}Manus[3], D. Mercer[3], J. A. G. Morris[5], J. V. Morris[5], D. Newton[4], A. O'Connor[4], R. Oedingen[1], A. G. Oganesian[7], P. J. Ottewell[3], C. N. Paterson[5], E. Paul[1], D. Reid[3], H. Rotscheidt[1], P. H. Sharp[5], S. Söldner-Rembold[1], N. A. Thacker[6], L. Thompson[6], R. J. Thompson[3], J. Waterhouse[3], A. S. Weigend[1], G. W. Wilson[4].

[1]Physikalisches Institut, Universität, Nussallee 12, D-5300 Bonn, Federal Republic of Germany
[2]CERN, CH-1211 Geneva 23, Switzerland
[3]Department of Physics, The University, Manchester M13 9PL, England
[4]School of Physics and Materials, Lancaster University, Lancaster LA1 4YB, England
[5]Rutherford-Appleton Laboratory, Chilton, Didcot, Oxon OX11 0QX, England
[6]Department of Physics, University of Sheffield, Sheffield S3 7RH, England
[7]Yerevan Physics Institute, Markavion St. 2, Yerevan, Armenia.

Abstract

Measurements are reported of inclusive $f_2(1270)$ and $f_0(975)$ production in γp, $\pi^{\pm}p$ and $K^{\pm}p$ collisions at photon beam energies of 65 to 175 GeV and hadron beam energies of 80 and 140 GeV. The f_2 and f_0 mesons were found at masses of 1.250 GeV and 0.961 GeV respectively. Inclusive f_2 production at low x_F was found to have a similar p_T dependence for each beam type, whereas an additional pion-exchange contribution was found for production by pions at high x_F. Cross sections are compared to those for $\rho^0(770)$ production and give no indication of a non-$q\bar{q}$ component in either f-meson state.

1 Introduction

The $f_2(1270)$ and $f_0(975)$ mesons have been observed in many previous experiments although with differences in their parameters and their interpretation. The f_2 seems to be a standard $q\bar{q}$ state but the width is still giving difficulties with a recent determination in pp [1] giving a value of 325 ± 55 MeV which was interpreted as evidence for a gluon content. New evidence for the existence of a spin zero enhancement under the $f_2(1270)$ has been reported in $\gamma\gamma \to \pi^0\pi^0$ and interpreted as an indication of an $f_0(1270)$ [2]. Thus further study of the $f_2(1270)$ region in inclusive mass spectra produced with different projectiles is valuable.

There is uncertainty in ascribing the $f_0(975)$ to the lightest $q\bar{q}$ scalar nonet. The $K_0^*(1430)$ and $a_0(980)$ are known and in the I=0 S-wave cross section there is a broad enhancement, $f_0(1400)$, that is largely elastic and the $f_0(975)$ which also couples to $K\overline{K}$. The $f_0(975)$ coupling to $K\overline{K}$ suggests that it contains an admixture of $s\bar{s}$ quarks; it has been interpreted as a $K\overline{K}$ molecule or a 4 quark state; see [3] for a review. Unconventional classification of $f_0(975)$ and $a_0(980)$ gets support from the possible observation of scalar $q\bar{q}$ objects by the partial wave analysis of $\eta\pi$ data by GAMS [4] and of $K_S^0K_S^0$ data by LASS [5], in which S-wave enhancements have been seen under the corresponding tensors $a_2(1320)$ and $f_2(1525)$.

Measurements are reported here, using data taken in experiment WA69 [6] at the CERN Omega spectrometer, of the inclusive production of $f_2(1270)$ and $f_0(975)$ in γp and $h^{\pm}p$ collisions; here $h^{\pm}$ denotes a mixture of $\pi^{\pm}$ and $K^{\pm}$ beams adjusted by means of beamline Cherenkov counters and software to a ratio of 2:1 in order to simulate the quark content of the photon [7]. A total of 20 million photon induced and 24 million hadron induced triggers (subdivided into 8 million at $\pm$ 80 GeV and 16 million at $\pm$ 140 GeV) were taken using a trigger which selected most of the hadronic total cross section. In the analysis, no dependence was found on the charge of the hadron beam and so all results presented are the sum of similar sized data sets taken with oppositely charged beams. These event samples yielded 96000 photoproduced and 250000 hadroproduced f_2 mesons, and 16000 photoproduced and 37000 hadroproduced f_0 mesons. The analysis reported here was similar to that described in [7], with the program TRIDENT [8] being used for event pattern recognition and reconstruction. In the photoproduced event sample, electromagnetic backgrounds were reduced by cutting events having equatorial tracks in the Omega magnetic field. Final elimination of electromagnetic contamination in the photon data and the minimisation of trigger biasses were achieved by requiring a minimum of four charged particles in the final state. Hence all elastic and the lower charged multiplicity part of the inelastic $\pi^+\pi^-$ production were suppressed.

The extraction of the f-mesons and measurement of their masses in the $\pi^+\pi^-$ mass distributions are described in section 2. In section 3 cross sections for $f_2(1270)$ production as functions of x_F and p_T are discussed as are total cross sections for production of the $f_0(975)$ meson. The reaction mechanisms for $f_2(1270)$ are discussed in section 4 and conclusions are given in section 5.

2 Masses and widths of the f-mesons.

Inclusive two-particle mass distributions were compiled for each of the beam types and for each of the energy ranges, assuming that all observed final state particles were pions. As an example, figure 1(a) shows the $\pi^+\pi^-$ mass spectrum for the total pion induced data (the corresponding photon and kaon induced data are similar). To measure f_0 and f_2 intensities, the $\pi^+\pi^-$ mass distributions in the mass range from 0.74 to 1.5 GeV were fitted using a function of the form:

$$\tilde{F}(m) = p_1 \cdot BG(m; p_2, p_3, p_4) + p_5 \cdot BW_{f_2}(m) + p_6 \cdot RES_\rho(m) + p_7 \cdot BW_{f_0}(m)$$

$$\text{with} \quad BG(m; p_2, p_3, p_4) = (m - 2m_\pi)^{p_2} \cdot \exp(-p_3 m - p_4 m^2),$$

$$BW(m) = \frac{m \cdot m_0 \cdot \Gamma(m)}{(m^2 - m_0^2)^2 + m_0^2 \cdot \Gamma^2(m)}, \qquad \Gamma(m) = \Gamma_0 \cdot \frac{2(\frac{m^2-4m_\pi^2}{m_0^2-4m_\pi^2})^{l+\frac{1}{2}}}{1 + \frac{m^2-4m_\pi^2}{m_0^2-4m_\pi^2}}$$

$RES_\rho(m)$ is the same Breit-Wigner form as was used in [7], i.e. skewed with a Söding like term to account for coherence effects with the background. The mass range was chosen so as to exclude the complex region on the lower side of the $\rho^0(770)$, and effects due to the $\pi^+\pi^-$ decay of the $\rho(1600)$. To account for the experimental resolution, the function $\tilde{F}$ was convoluted with the resolution function $G(\delta m; m)$ extracted from the momentum errors of the tracks as given by the reconstruction program. The parameters p_i of the resulting function

$$F(m) = \int G(m - m'; m')\tilde{F}(m')dm'$$

were fitted using the program MINUIT [9].

Figure 1(a) shows a fit to the pion data with the masses, widths, and spins quoted by the particle data group[10] (m_{f_2} = 1274 MeV, Γ_{f_2} = 185 MeV, $l_{f_2} = 2$; and m_{f_0} = 975.6 MeV, Γ_{f_0} = 33.6 MeV, $l_{f_0} = 0$). This fit has a χ^2-probability of 4.7 per degree of freedom. The significance for the f_0 signal is approximately 9 standard deviations in the π data, 5 in the K data and 8 in the photon data. The f_2, but not the f_0 signals are much more pronounced at high x_F as seen in figure 1(b) which shows the $\pi^+\pi^-$ mass spectrum for π pairs from figure 1(a) with $x_F > 0.7$. In order to investigate the fits to the f signals in more detail, all contributions, except those from the f_2 and f_0, were subtracted; figure 1(e) shows the resulting distribution. Both resonances appear to be shifted towards lower mass values than those given by the Particle Data Group [10]. This effect is also seen in the corresponding plot for the photon and kaon induced data (figures 1(c) and (g)). Independent fits to the photon and pion data with variable f-meson masses yielded consistently $m_{f_2} = 1250 \pm 3$ MeV and $m_{f_0} = 961 \pm 3$ MeV. Hence the masses were fixed at these values throughout the rest of the analysis. Corresponding fits are shown in figures 1(d) (photon data), 1(f) (pion data) and 1(h) (kaon data). The overall χ^2 per degree of freedom was typically 1.3 for the fits to the photon and pion data. A possible interpretation of these mass shifts is discussed below.

Tests of the stability of these results have been made. Systematic shifts in the mass determination due to the detector are excluded by the observation that the $K^{*0}(892)$ and $\phi(1020)$ mesons were observed precisely at their nominal mass values [11]. The replacement of a skewed ρ^0 shape by a normal Breit-Wigner ρ^0 increased the fitted mass of the $f_0(975)$ to 966 MeV and its intensity by 25%, had a negligible effect on the f_2 parameters, increased

the overall χ^2 per degree of freedom to 2.3 and made the fits in the ρ^0 region much worse. Allowing an additional cubic term in the background, such as was found necessary in [7], increased the fitted intensity of f_2 by 2%, but made a negligible change to the χ^2 per degree of freedom, or the overall shape or other f_0 or f_2 parameters. Thus, although the backgrounds in the region of both f-meson peaks are large, the f-meson parameters are stable to the form of the background. Hence it appears unlikely that the mass shifts are caused by errors in the background estimation.

The yield of $\rho^0(1600)$ in the $\pi^+\pi^-$ mass spectra around 1600 MeV was far too small to influence the f_2 signal. There is no indication for a $\rho^0(1250)$ in the elastic data of the reaction $\gamma p \rightarrow \pi^+\pi^- p$ [12] or $e^+e^- \rightarrow \pi^+\pi^-$ [13]. Hence the possible contribution of 1^{--} resonances in the immediate vicinity of the f-meson peaks has been neglected.

Final state particle identification was not used in this analysis, and so the $K^\pm\pi^\mp$ decay of the $K_2^*(1430)$ reflects into the $\pi\pi$ mass spectrum with a peak at about the f_2 mass. This is potentially important in the kaon data where leading production of the K_2^* is expected. The magnitude of the effect has been measured by assigning the kaon mass to one of the charged particles and fitting the K_2^* in the resulting mass spectrum. The yield due to the K_2^* reflection (shown as the shaded area in figure 3(f)) corresponds to less than a 15% K_2^* contamination of the f_2 signal in the kaon induced data. This contamination was found to be negligible in the photon and pion induced data.

The existence of a spin zero bump under the f_2 has been reported in $\gamma\gamma \rightarrow \pi^0\pi^0$ and interpreted by [2] as an indication for an $f_0(1250)$. This state could be present here and could contribute to the low mass observed for the f_2. A fit allowing such a state in addition to a standard mass f_2 is satisfactory but assigns the whole of the peak to such an f_0. As shown below there is good evidence, at least at high x_F in pion production, that the 1250 MeV peak in the present data has a dominantly high spin component. A contribution to the f_2 peak from a $\pi^+\pi^-$ decay of another resonance at about this mass cannot be excluded. An alternative, and plausible, explanation of the mass shifts found here is that they are due to interference between the f resonances and the background; such an explanation was used successfully to describe ρ^0 meson production in [7]. Although in general interference effects can alter the total area under a peak, so that neglecting them may introduce errors in a cross section measurement, the error due to the shifts reported here is small. Interference effects in f_0 production in the quasi two-pomeron exchange $pp \rightarrow \pi^+\pi^-$ and $pp \rightarrow K^+K^-$ at 300 GeV have been observed by WA76 [14], but this cannot be directly compared with the present work.

3 Cross sections for f-meson production

The Monte Carlo program HERWIG [15] was used as an event generator to provide a sample of f_2 mesons for the determination of the experimental acceptance over the x_F-p_T grid. This program produced, by default, tensor mesons in the final state of the hadronization procedure. It was used in its default mode, and the f_2 was taken at its nominal mass, decaying isotropically into $\pi^+\pi^-$. The f_2 width given by [10] was applied. The Monte Carlo events were processed through a simulation chain taking account of the detector, trigger, and data selection as in [7], and the number of f_2-mesons extracted from the resulting mass spectra. The acceptance was then calculated as the ratios of reconstructed to input numbers of f_2 per

Beam type	Energy	σ [μb]
γ	65 - 110 GeV	5.18 $\pm$ 0.24
γ	110 - 175 GeV	4.62 $\pm$ 0.28
γ	65 - 175 GeV	5.06 $\pm$ 0.21
π	80 GeV	1186 $\pm$ 45
π	140 GeV	1306 $\pm$ 43
K	80 GeV	386 $\pm$ 44
K	140 GeV	435 $\pm$ 30
h	80 GeV	919 $\pm$ 32
h	140 GeV	1016 $\pm$ 35
h	80/140 GeV	967 $\pm$ 28

Table 1: Total cross sections for inclusive f_2 production in the range $-0.1 \leq x_F \leq 1$ and $p_T \leq 2$ GeV. The quoted errors exclude the normalisation uncertainty of $\pm 15\%$ but include a $\pm 2\%$ estimate of the error due to the choice of background parametrisation.

x_F and p_T bin. The acceptance varied by less than a factor of 2 over the whole x_F and p_T range and agreed well in magnitude and shape with the acceptance for ρ^0 mesons deduced in [7]. Its dependence on the beam energy was weak.

Cross sections for f_2 production were evaluated for bins of 0.4 GeV in p_T over the range from 0 to 2 GeV/c, and of 0.2 or 0.3 in x_F over the range from -0.1 to 1.0. Two ranges of beam energy were taken separately: *low* energy, $65 < E_\gamma < 110$ GeV and $E_{had} = 80$ GeV; and *high* energy, $110 < E_\gamma < 165$ GeV and $E_{had} = 140$ GeV. A correction for the branching ratio of $f_2 \rightarrow \pi^+\pi^-$ of 56.7% has been made. Figures 2(a-f) show the differential cross sections, $d^2\sigma/dx_F dp_T$, for f_2 production for each combination of beam particle type and beam energy. The fit errors on each x_F-p_T bin at low p_T are typically $\pm 20\%$, $\pm 20\%$ and $\pm 30\%$ for γ, π and K beams respectively. In addition, there is a $\pm 15\%$ normalisation uncertainty in all data. The total cross sections, integrated over x_F and p_T are given in table 1.

Figures 2(a-f) show that different projectiles give rather different distributions at high x_F. Figures 3(a-f) give the x_F projection, and the histograms on 3b and 3f show the prediction of HERWIG normalised to the data. The shaded histogram in figure 3(f) shows the amount of $K_2^*(1430)$ contamination in the f_2 signal.

The ratios of production cross sections for π and K beams give information on the nature of states. At high x_F the ratio is determined by the possible meson exchange mechanisms, whereas at lower x_F, near zero, the ratio gives information on the quark or gluon content of the state. For u/d quark states the ratio would be equal to 2, by valence quark counting. This value is likely to be reduced slightly by contributions from sea quarks or gluons. If the state contains strange quarks (e.g. a $K\overline{K}$ molecule) the ratio would be expected to fall even further. Figure 4 shows this ratio for f_2 and ρ^0 production as functions of x_F, indicating that the shapes are consistent. Some systematic errors are possible because of the somewhat different shapes of the background distributions for π and K beams and the results are thus consistent with being equal and having a value close to 2 in the region $x_F < 0.5$. The rise at higher x_F presumably results from meson exchange contributions in this region.

The corresponding ratio for $f_0(975)$ production is less well determined but is again consistent with a value of 2, and therefore points to a u/d quark interpretation of the

Beam type	$\sigma(\rho^0)$	$\sigma(f_2)$	$\sigma(f_0)$
γ	17.0 ± 0.2	5.06 ± 0.21	1.18 ± 0.15
π	4004 ± 50	1250 ± 45	180 ± 20
K	2001 ± 90	410 ± 36	109 ± 20

Table 2: Meson production cross sections in μb. Errors are statistical and neither an overall normalisation error of $\pm 15\%$ nor systematic errors due to the parametrisation are included.

f_0 meson. In an earlier photoproduction experiment using the same spectrometer [16], a standard u/d quark structure was favoured for the $a_0(980)$, the apparent isovector partner of the f_0 in the scalar octet: inclusive photoproduction of charged a_0 (with a subsequent decay into $\eta\pi^{\pm}$) was observed with a large cross section and was found to fit well into a $q\bar{q}$ production scenario involving light quarks only.

Total production cross sections (with a minimum observed charged multiplicity of 4 – see section 2) for ρ^0 (from [7]), f_2, and f_0 are given in table 2. (A branching ratio for $f_0 \to \pi^+\pi^-$ of 52.1% has been assumed.) It should be noted that the ratios of f_0 and f_2 total cross sections cannot be simply interpreted because of the additional f_2 production mechanism at large x_F which is discussed below. There was insufficient data to determine differential f_0 production cross sections with respect to x_F or p_T.

4 Production dynamics for f_2 mesons

As a comparison of photon and hadron induced data in the central region, figure 5 shows the differential cross section, $d\sigma/dp_T$, for a subset of the data where a cut on $x_F(f_2) < 0.5$ has been applied. The corresponding plot for high x_F (not shown) is similar. The lines in figure 5 correspond to a fit of the form

$$\frac{d\sigma}{dp_T} = a\, p_T \exp(-b\, p_T^2)$$

to the data points. The fitted values of the parameter b for the six data samples are all consistent with each other and give an average value, $b = 2.0 \pm 0.1$ GeV^{-2}. Since the f_2 state is well separated in rapidity from the projectile, it is not expected to be significantly spin aligned and decay angular distributions of the f_2 decay products would be expected to be isotropic. This angular distribution (not shown) is indeed observed to be isotropic for each beam type.

At larger x_F ($x_F > 0.7$), there is a substantial yield with a strong angular dependence in the hadron-induced data. This suggests an additional mechanism in hadro-production and also confirms that the object seen at a mass of 1250 MeV at high x_F is dominantly a high spin object such as the f_2. Only pion induced data were used for this analysis because of the K_2^* contamination in the kaon induced data. The angular distribution for a pion from the f_2 decay, integrated over the azimuthal angle, is given by [17]:

$$W(\cos\theta) \propto \left\{ \rho_{22} \sin^4\theta + \rho_{11} \sin^2 2\theta + 3\rho_{00} \left(\cos^2\theta - \frac{1}{3} \right)^2 \right\} \qquad (1)$$

	these data			[18]			OPEA
ρ_{00}	0.66	$\pm$	0.02	0.93	$\pm$	0.07	0.85
ρ_{11}	0.27	$\pm$	0.01	0.26	$\pm$	0.02	0.07
ρ_{22}	-0.10	$\pm$	0.01	-0.22	$\pm$	0.02	0

Table 3: Measured spin density matrix elements for f_2 at $x_F > 0.7$ (π data, high energy). The errors are purely statistical.

where ρ_{ij} are the spin-density matrix elements and the polar angle θ is that of the decay π^+ with respect to f_2 momentum in the overall center of mass system. This has been successfully applied [18] to the description of $d\sigma/d\theta(\pi^- p \to f_2 n)$ at a π^- energy of 8 GeV. In the present analysis it leads to a fit of the data as described by the dotted curve figure 6, with results listed in table 3. The fit was restricted to the range $\pi/10 < \theta < 9\pi/10$ so as to avoid uncertainties in the acceptance at extreme values of θ.

The OPEA-model (one pion exchange with absorption [18]) predicts a preponderant ρ_{00} contribution to $W(\cos\theta)$ in equation 1 which is seen in the fourth column of table 3. Table 3 also gives the results of [18] and of this experiment. In this experiment the f_2 is found to be dominantly produced at low p_T, i.e. in the regime of one pion exchange. The measurement of a non-vanishing ρ_{22} indicates the existence of other exchange contributions or of a small contribution from a lower spin resonance (e.g. the $f_0(1250)$ suggested by [2] superimposed on the f_2). The measured p_T distribution at large x_F can be described by a triple Regge ansatz including a_2-exchange. Reference [7] argues that such a mechanism can be parametrized by

$$\frac{d^2\sigma}{dtd(M_X^2/s)} \propto G_{\pi\pi P}(t) \cdot \left(\frac{s}{M_X^2}\right)^{2\alpha_\pi(t)-1} + G_{a_2a_2P}(t) \cdot \left(\frac{s}{M_X^2}\right)^{2\alpha_{a_2}(t)-1}, \qquad (2)$$

$$\text{where} \quad G_{\pi\pi P} = A\frac{\exp(-6t)}{(t-m_\pi^2)^2} \quad \text{and} \quad G_{a_2a_2P} = B.$$

The data are not sensitive to the value of the exponent in the above expression for $G_{\pi\pi P}$ and values up to 9 show little variation in the quality of the fits. The parameters A and B were determined by fitting the data for $\pi p \to f_2 X$ (high energy, $x_F > 0.7$) to equation (2) and the result is shown on figure 7(a). The curve on figure 7(b) shows the consequent prediction of the spin dependent contribution according to equation 2 superposed on the data already shown on figure 3d .

5 Conclusions

Inclusive $\pi^+\pi^-$ mass distributions have been studied in photo- and hadro-production, and f_2 and f_0 meson production have been measured. The masses of the peaks have been found to be lower than previously reported, at 961 and 1250 MeV, whereas the widths agree well with previous work. The natural explanation of the mass shifts is interference with non-resonant (or possibly resonant) backgrounds. Cross sections for $f_2(1275)$ production were measured as functions of three kinematical variables: x_F, the transverse momentum p_T with respect to the beam direction and the polar decay angle θ of the decay π^+ with respect to the f_2-momentum in the overall center of mass system. The cross sections are interpreted in terms

of different production mechanisms in different x_F regions. Central production is isotropic and rather independent of the beam type. The ratio of production by pion and kaon beams are consistent with a $q\bar{q}$ interpretation of the bump. Forward production, with a pion beam, shows strong backward and forward peaks for the decay pions relative to the beam direction. This supports the interpretation of the dominant contribution to the bump at 1250 MeV being due to a high spin state such as the f_2 rather than the proposed $f_0(1250)$. The high x_F data are interpreted using the phenomenology of the triple Regge picture. There remains a possibility that the object produced at low x_F at a mass of 1250 MeV is not the same as the peak seen at higher x_F, although the similar masses and the plausible explanation given above make this unlikely. Corresponding high x_F effects for kaon production of f_2 mesons are not expected to be detectable because of the relative magnitude of the coupling constants.

The ratios of $f_0(975)$-meson total production cross sections for π and K beams compared with those for the corresponding ρ^0 production suggest that the f_0-meson is a normal $q\bar{q}$ state.

Acknowledgements
BMFT-Foerderkennzeichen 05-5BN17I(4) (Fed. Rep. Germany) and SERC (U.K.) helped financially and this is gratefully acknowledged. All the technicians and the CERN OMEGA and beam line groups made vital contributions. The computer centres at Bonn (RHRZ), RAL, and CERN have been very generous in their support.

References

[1] A. Breakstone et al., Z. Phys. C48 (1990) 569

[2] J. K. Bienlein et al., DESY-91-145

[3] B. Diekmann, Phys. Rep. 159 (1988) 101

[4] D. Alde et al., Phys. Lett. B205 (1988) 397

[5] D. Aston et al., Nucl. Phys. B256 (1985) 525

[6] R.J. Apsimon et al., Z. Phys. C43 (1989) 63

[7] R.J. Apsimon et al., Z. Phys. C53 (1992) 581

[8] J.C. Lassalle et al., CERN-DD/EE/79-2, and NIM 176 (1980) 371

[9] F. James, M. Roos, CERN Pool Program D506 (1989)

[10] Particle Data Group, Phys. Lett. B239 (1990) 1

[11] R.J. Apsimon et al., Comparison of photon and hadron induced production of ϕ, K^{*0} and $\overline{K}^{*0}$ mesons in the energy range from 65 to 175 GeV, in preparation,
F.-D. Gebert, PhD thesis, Bonn (1992)

[12] D. Joseph, BONN-IR-89-07

[13] L.M.Barkov et al., Nucl. Phys. B256 (1985) 365
D. Bisello et al., Phys. Lett. B220 (1989) 321

[14] Conf report from 1990 St.Goar conf in NPB(Supp)21(1991)49.

[15] G. Marchesini, B. R. Webber, CERN Pool Program W5037 (1989)

[16] M. Atkinson et al., Phys. Lett. 138B (1984) 459

[17] H. Hoegasen et al., Nuovo Cimento 42 (1966) 323,
J.D. Jackson, Nuovo Cimento 34 (1964) 1644

[18] J.A. Poirier et al., Phys. Rev. 136 (1967) 1462

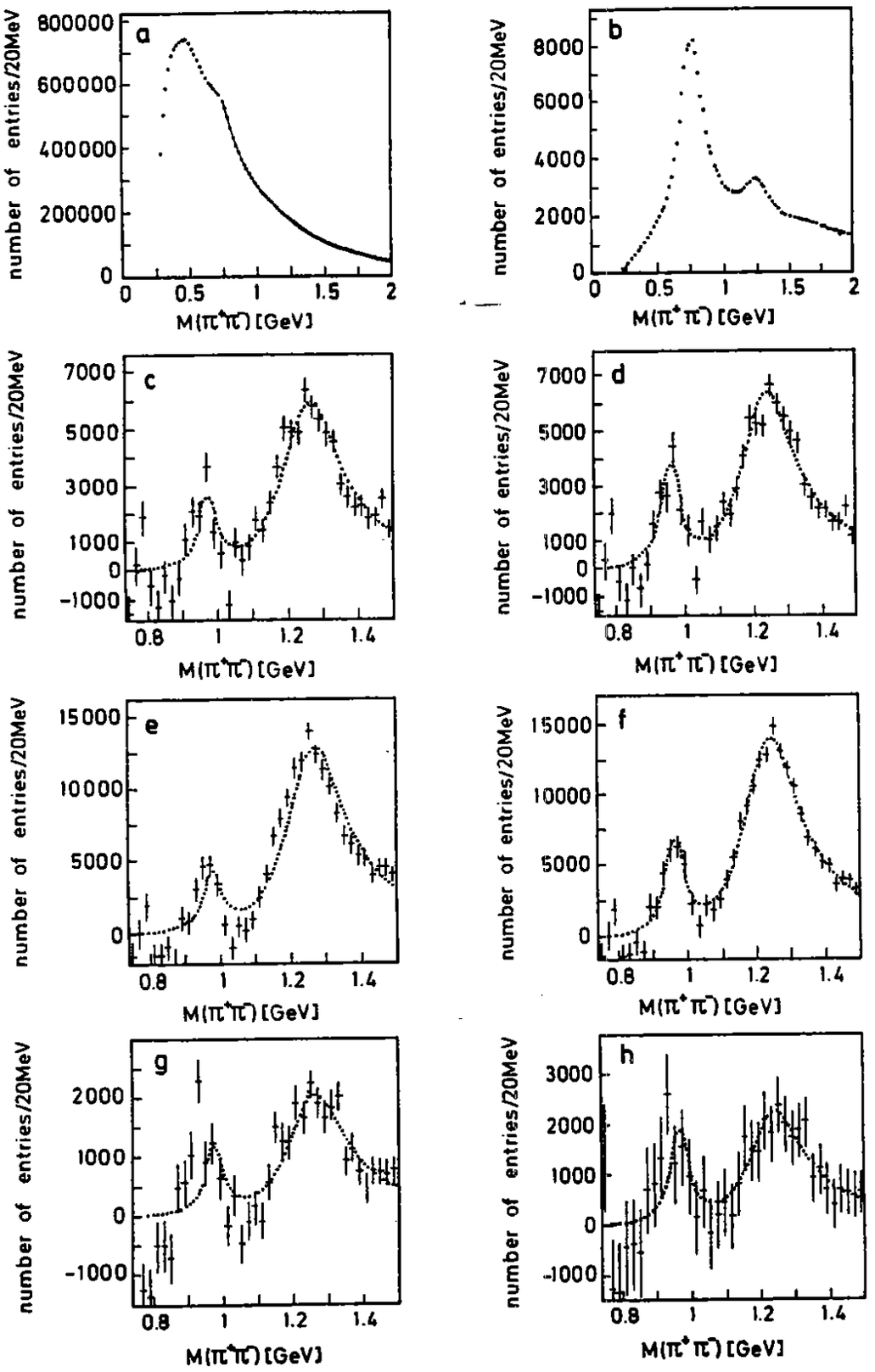

Figure 1: Invariant $\pi^+\pi^-$ mass distributions for: (a) pion induced data summed over all x_F and p_T with the fit described in the text (f_2 and f_0 at their nominal masses), the photon data are very similar; (b) the subset of the pion induced data where the $\pi^+\pi^-$ combination is at $x_F > 0.7$; (c) photon data after subtraction of fitted background; (d) as (c) but with $m_{f_2} = 1.250$ GeV and $m_{f_0} = 0.961$ GeV; (e) as (c) for pion induced data; (f) as (d) for pion induced data; (g) as (c) for kaon induced data; (h) as (d) for kaon induced data.

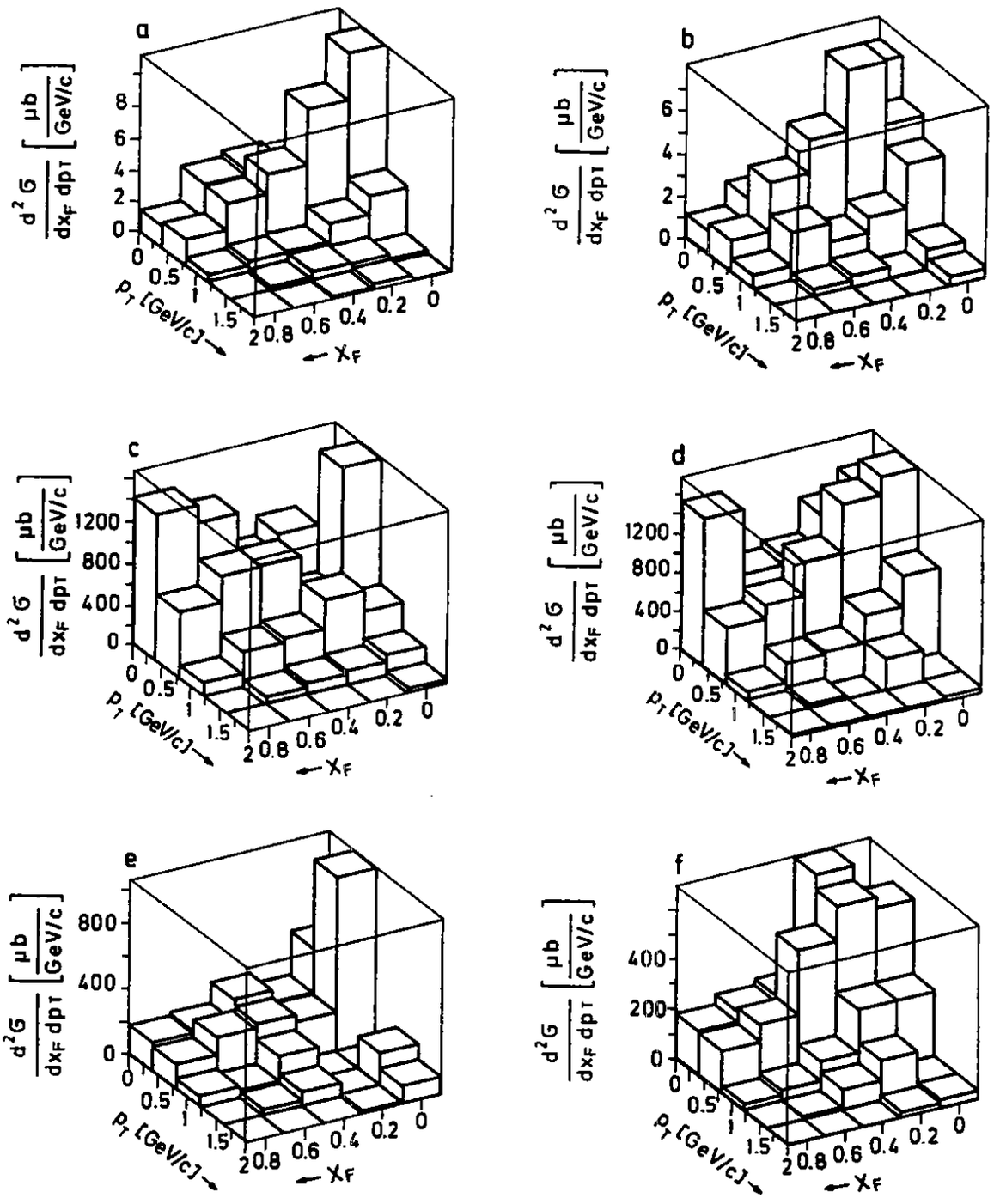

Figure 2: Inclusive cross section for f_2 production vs x_F and p_T: (a) photon beam, low energy; (b) photon beam, high energy; (c) pion beam, low energy; (d) pion beam, high energy; (e) kaon beam, low energy; (f) kaon beam, high energy. Note that the highest x_F bin includes all data from 0.7 to 1.0.

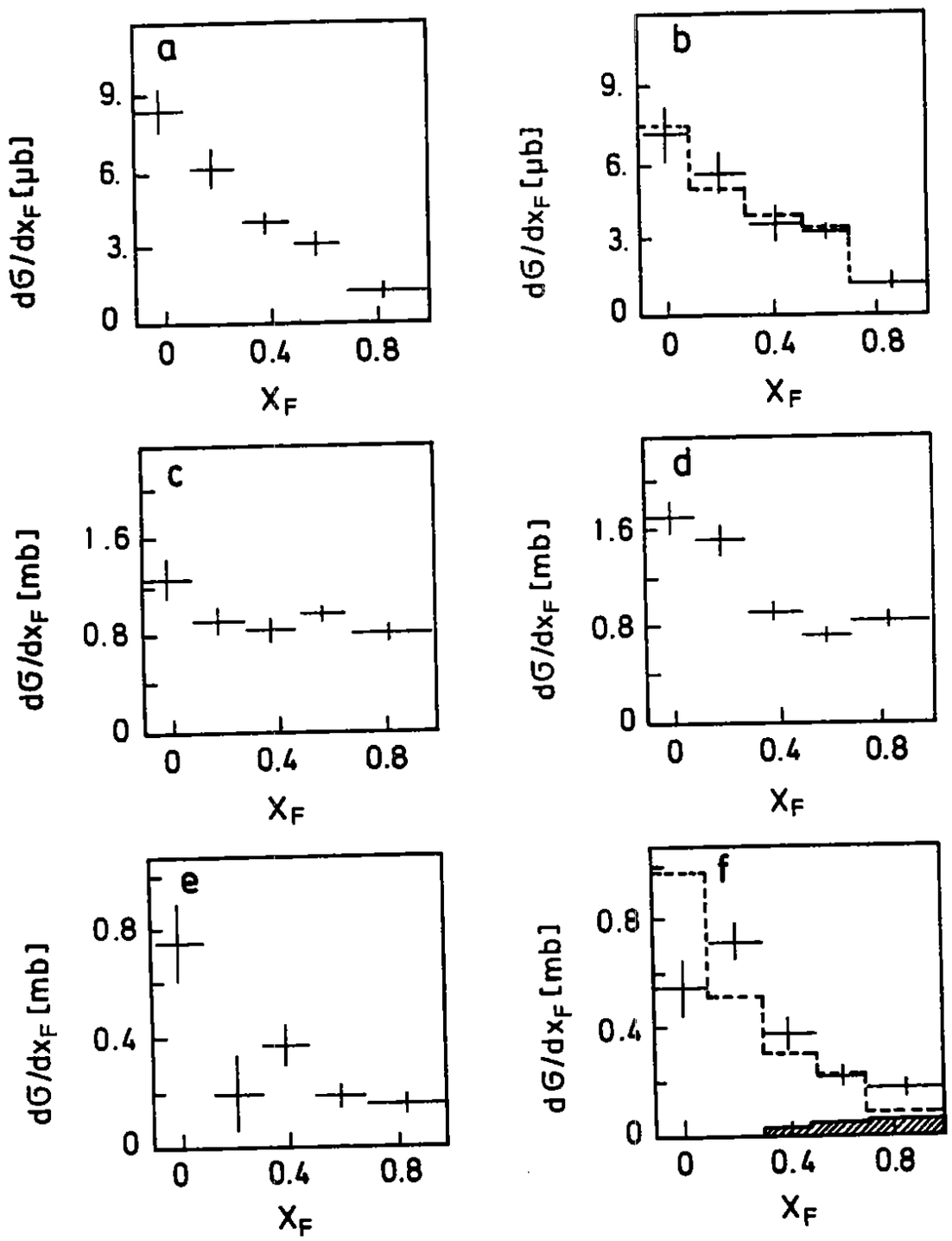

Figure 3: Inclusive cross section for f_2 production vs x_F: (a) photon beam, low energy; (b) photon beam, high energy; (c) pion beam, low energy; (d) pion beam, high energy; (e) kaon beam, low energy; (f) kaon beam, high energy. The histograms show the HERWIG predictions (see text) and the shaded area indicates the amount of K_2^* contamination.

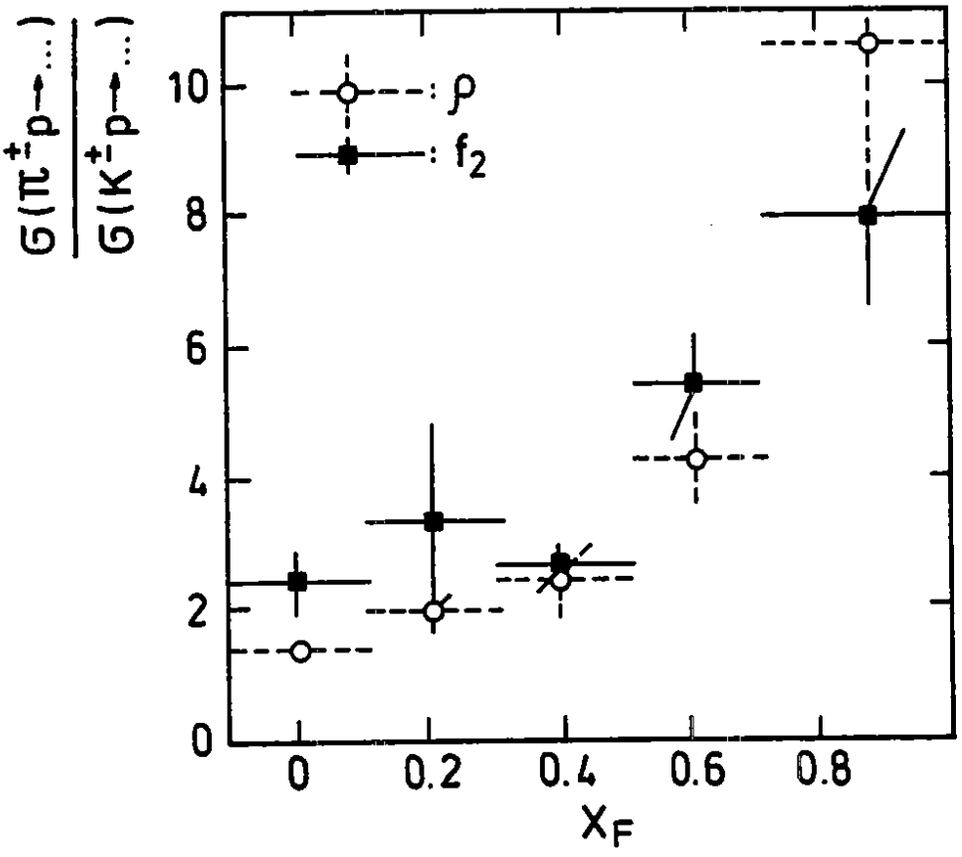

Figure 4: Ratios of cross sections for π and K beams as a function of x_F for $f_2(1270)$ (shown as black squares) and ρ^0 (shown as open circles). Data have been corrected for the K* reflection.

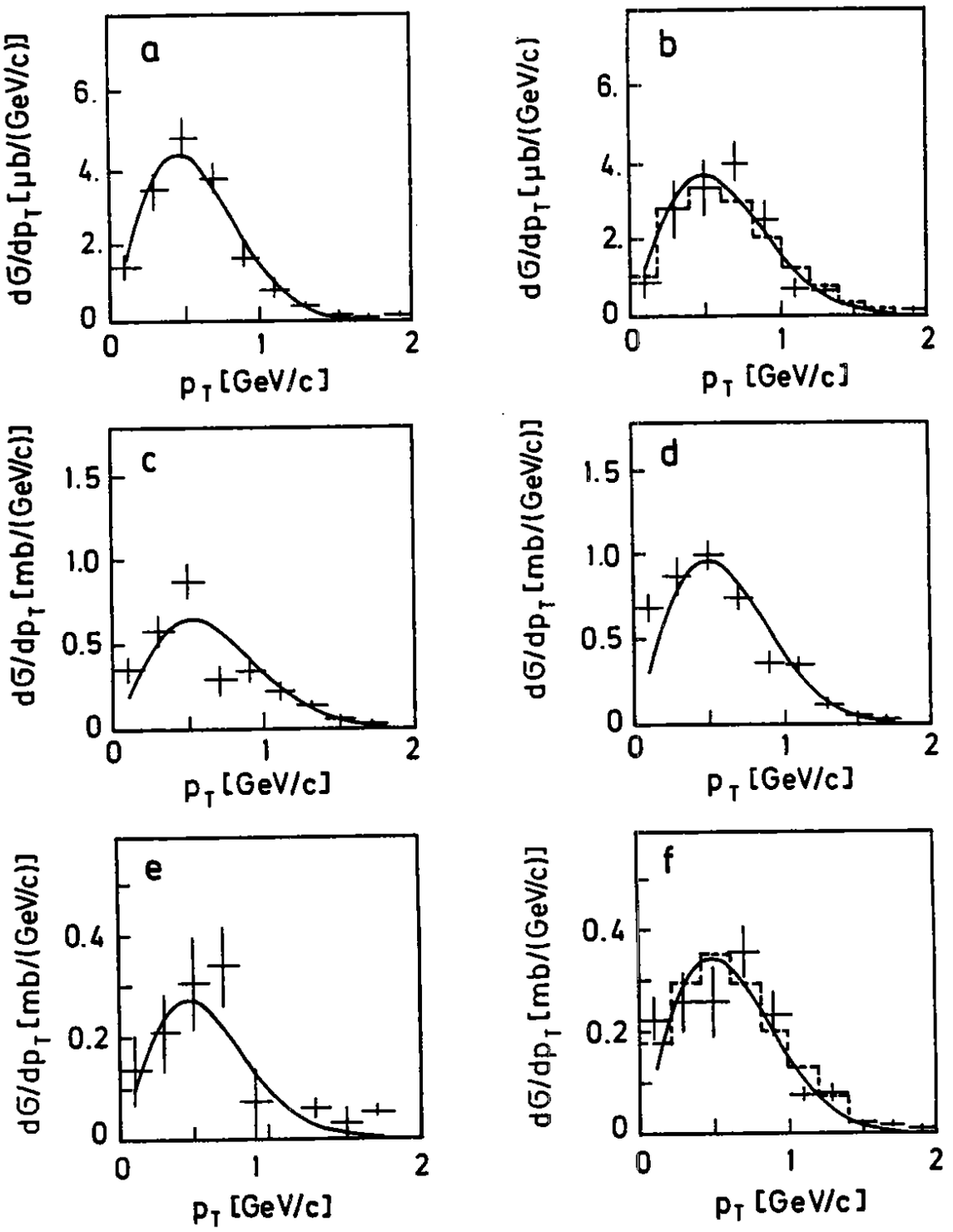

Figure 5: Inclusive cross section for f_2 production vs p_T for $x_F(f_2) < 0.5$: (a) photon beam, low energy; (b) photon beam, high energy; (c) pion beam low energy; (d) pion beam, high energy; (e) kaon beam, low energy; (f) kaon beam, high energy. The line shows the fit to an exponential form, the dashed histogram corresponds to the HERWIG prediction.

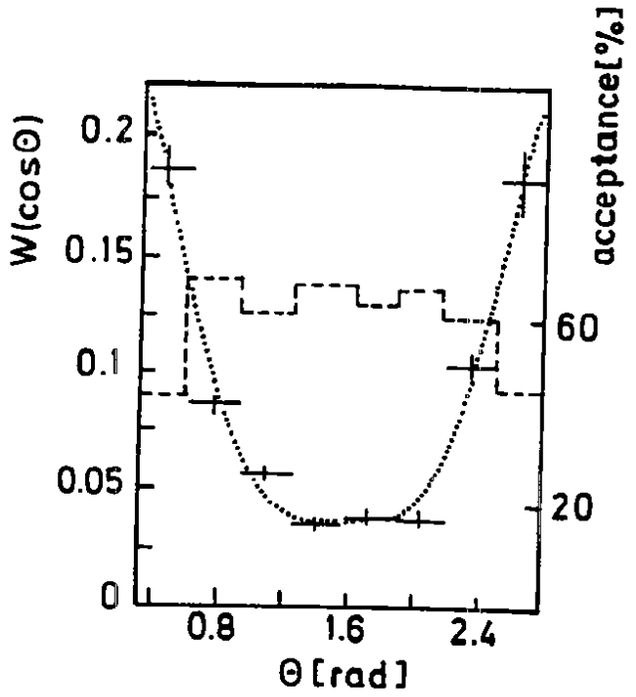

Figure 6: Decay angular distribution, $W(\cos\theta(f_2 \to \pi^+\pi^-))$, from pions at high energy. The dotted curve corresponds to the fit to equation (1) and the dashed histogram shows the acceptance.

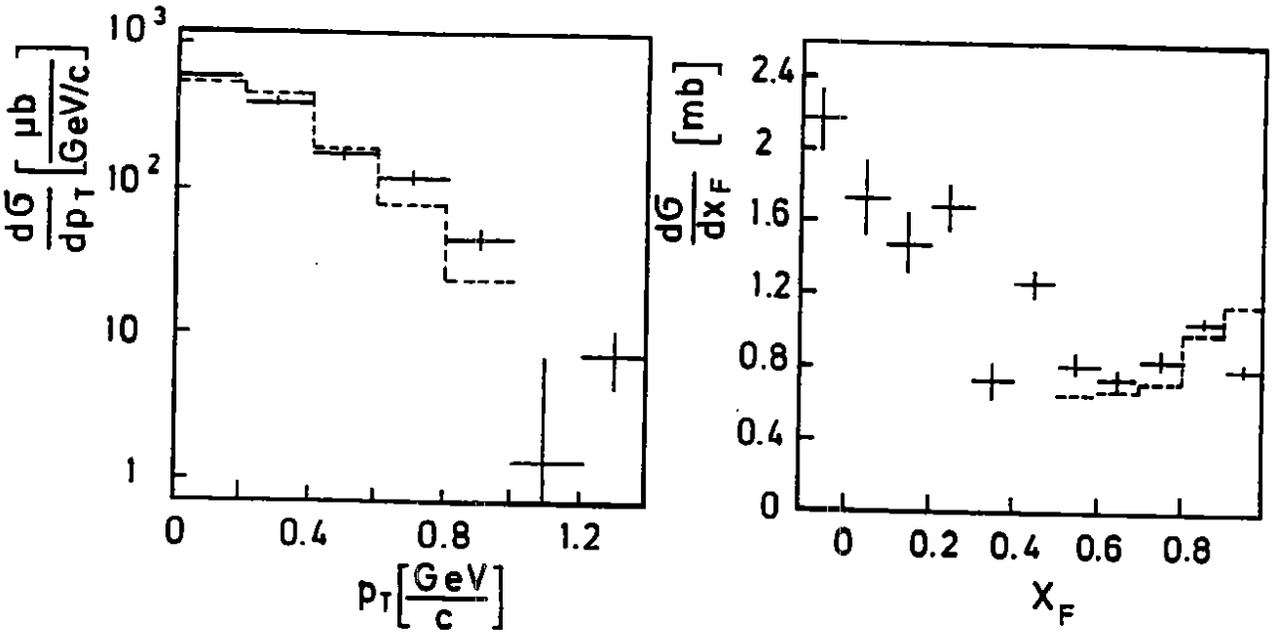

Figure 7: (a) Differential cross section, $d\sigma/dp_T(\pi p \to f_2 X)$ for $x_F(f_2) > 0.7$ (the dashed histogram corresponds to the triple Regge fit); (b) $d\sigma/dx_F(\pi p \to f_2 X)$ (the curve shows the triple Regge fit).